



Palaeo- and rock magnetic investigations of Late Quaternary sediments from the Upper Congo deep-sea fan: on the difficulty in obtaining palaeomagnetic secular variation records from low latitudes

Ute Frank¹ · Norbert R. Nowaczyk¹ · Thomas Frederichs² · Jiabo Liu¹ · Monika Korte¹ 

Received: 23 January 2018 / Accepted: 20 September 2018 / Published online: 1 October 2018
© Springer-Verlag GmbH Germany, part of Springer Nature 2018

Abstract

We report here on results of palaeo- and rock magnetic investigations of two sediment cores from the Upper Congo deep-sea fan. The sediments have a high organic content and contain a heterogeneous Fe-mineral assemblage with biogenic magnetite and detrital (Ti-)magnetite as the main magnetic carrier minerals. Pyrite, hematite, and Fe-oxyhydroxides were identified by comparing high-temperature magnetic susceptibility curves with those from Fe-minerals of known composition. According to AMS ¹⁴C dates, the 6.8 m-long profile spans the last 37 kyr. Sediments older than 20 ka are affected by reductive diagenesis that has led to a loss of the fine-grained magnetic mineral fraction. Sediments younger than 20 ka have stable magnetizations. Characteristic remanent magnetization records of inclination and declination were obtained for each core. There is a little agreement between these records, modelled curves, and other sediment records from Equatorial Africa, so no composite record could be established. The cores are not ideal relative palaeointensity recorders and estimates using different normalizers did not yield consistent signals from both cores. Normalization methods used for relative palaeointensity estimation were not developed for sediments that contain large amounts of ultra-fine-grained biogenic magnetite; therefore, the relative palaeointensity estimates should be considered with caution. However, in view of the incoherent picture given by the scarce available palaeointensity information from the region off South-West Africa, the GeoB6517-2 record may provide a tentative relative palaeointensity record for comparison, at least for the past 10 kyr.

Keywords Magnetic mineralogy · Palaeomagnetic secular variation · Palaeointensity · Late quaternary · Upper Congo deep-sea fan

Introduction

It is now a common procedure in palaeomagnetic investigations to test the validity of the reconstructed signal obtained from sediments, volcanic rocks, and archaeological material

against a set of geomagnetic field models (e.g., Barletta et al. 2010; Gallet et al. 2015; Kissel et al. 2015; Bourne et al. 2016). For areas where the database for modelling is well stocked, such as Europe or North America, this method is often successful and might be justified. However, in regions where data coverage is sparse, the validity of the models is restricted, because they cannot be better than the input data, and the model output should be considered with caution. Thus, new records of geomagnetic palaeosecular variation (PSV) and relative palaeointensity (RPI), especially for low latitudes and the southern hemisphere, are needed to fill data gaps.

The ideal material for such studies would be long, mostly lithogenic sediment cores with continuously high sedimentation rates, containing sufficient amounts of fine-grained (Ti-)magnetite as the dominant magnetic

Electronic supplementary material The online version of this article (<https://doi.org/10.1007/s00531-018-1653-3>) contains supplementary material, which is available to authorized users.

✉ Monika Korte
monika@gfz-potsdam.de

¹ GFZ German Research Centre for Geosciences, Telegrafenberg, 14473 Potsdam, Germany

² Faculty of Geosciences, University of Bremen, Klagenfurter Strasse, 28359 Bremen, Germany

carrier mineral and unaffected by diagenesis. Most sediment cores recovered from low latitudes and the southern hemisphere are obtained mainly for palaeoclimatic studies, which target sites with characteristics that are less ideal for palaeomagnetic purposes. Abundant organic matter and rapid sedimentation changes, for example, are not ideal for reconstructing PSV and RPI records. Here, we present results from two marine sediment cores from the Congo deep-sea fan. Although neither of the two cores possesses ideal characteristics for palaeomagnetic studies, a lack of alternatives means that they currently provide our best information about South Atlantic Holocene palaeomagnetic variations.

Material

The studied sediment cores were recovered from two different sites on the Upper Congo deep-sea fan (Fig. 1). During Ocean Drilling Program (ODP) Leg 175, “Benguela Current” Hole 1076D ($5^{\circ}4.13'S$, $11^{\circ}6.12'E$) was drilled at 1401 m water depth (Wefer et al. 1998b), whereas core GeoB6517-2 ($5^{\circ}37.0'S$, $11^{\circ}19.9'E$) was recovered from 642 m water depth during RV *Meteor* cruise M47/3 (Spieß and Cruise 2002). Core GeoB6518-1 ($5^{\circ}35.3'S$, $11^{\circ}13.3'E$) from the same cruise provides the chronology for this study, but it is from a water depth of 962 m. GeoB6517-2 and GeoB6518-1 were both recovered within the freshwater plume in front of the Congo River mouth (Spieß and Cruise 2002), whereas ODP Hole 1076D is situated at its NE periphery (Wefer et al. 1998a). The fan sediments are

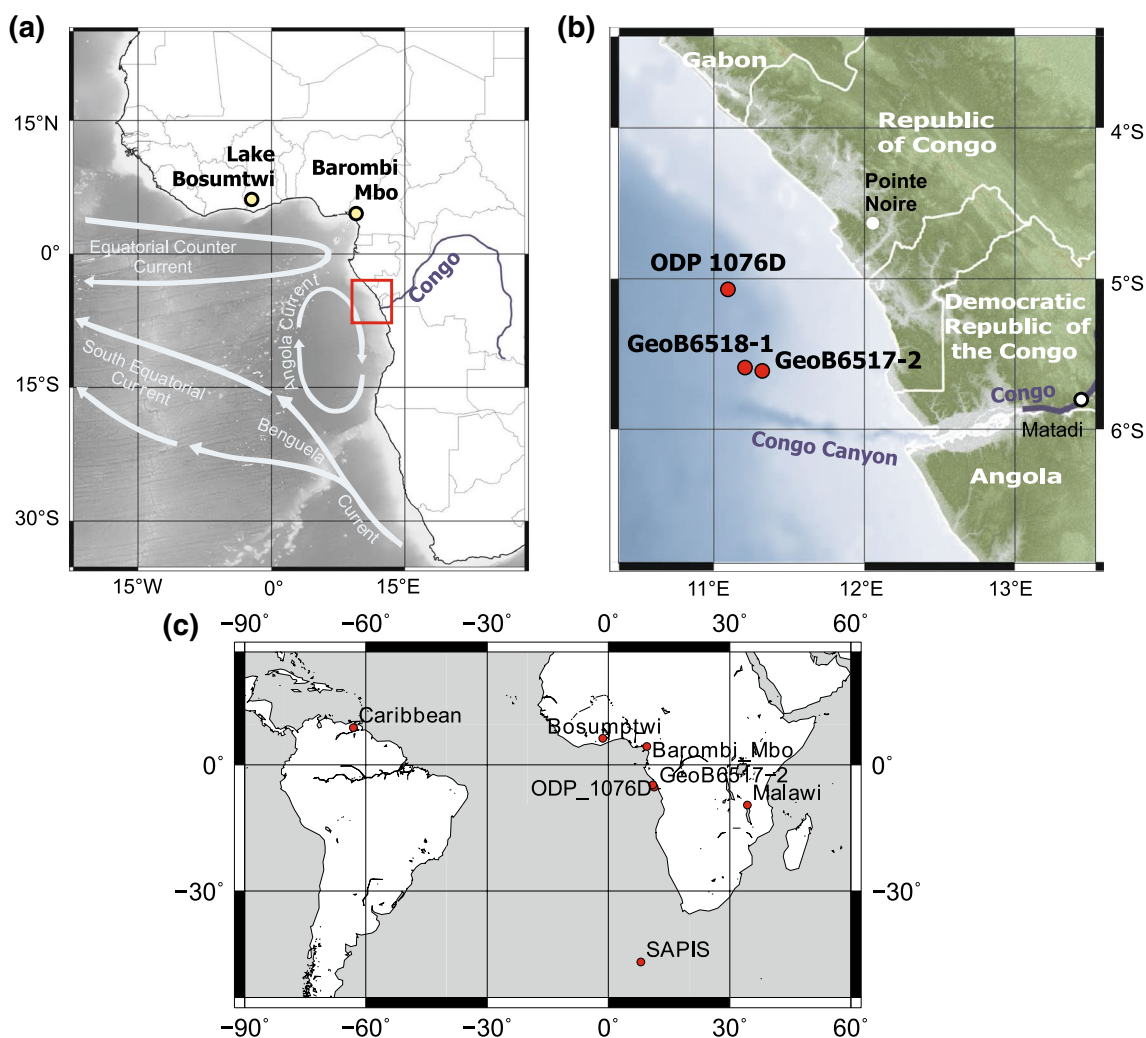


Fig. 1 Geographical position of the coring area within the South Atlantic current systems offshore of tropical West Africa (a) and locations of the cores relative to the Congo River mouth (b). The locations of additional sites referred to in the text are shown in panel c

a mixture of reworked shelf material and pelagic sediments with hematite and hematite-coated quartz, contributed by the Congo (formerly known as the Zaire) River (Heezen et al. 1964), and authigenic as well as reworked pyrite (Vreumingen 1984; Eisma et al. 1978). The sediment matrix is composed of organic carbon-rich olive grey and grey clays, with an average total organic carbon (TOC) content of about 3 wt% and a CaCO_3 content of about 4 wt% (Weijers et al. 2009; Wefer et al. 1998b).

Methods

Continuous magnetic susceptibility logs were measured on the archive halves of cores GeoB6518-1 and GeoB6517-2 in 1 cm increments with a Bartington Instruments MS2F sensor integrated in a split core logging system at the Faculty of Geosciences, University of Bremen. Core GeoB6517-2 and the uppermost 550 cm of core ODP 1076D were then sub-sampled continuously with plastic boxes ($20 \times 20 \times 15$ mm) that were pushed into the sediment surface at 20 mm intervals. A filled sample was removed carefully before the next sample was pushed into the sediment, yielding continuous coverage by the samples. All samples were weighed and the low-field

magnetic susceptibility κ_{LF} was measured with a Multi-Function Kappabridge MFK-1A (AGICO Brno) at 976 Hz. Palaeomagnetic investigations included the measurement and stepwise alternating field (AF) demagnetization of the natural remanent magnetization (NRM) with a fully automated cryogenic 2G Enterprises 755 superconducting rock magnetometer (SRM) based on DC-SQUIDS with a noise level of about 10^{-6} Am^{-1} for a 6 cm^3 sample volume. AF demagnetization was carried out in ten steps up to a peak field of 100 mT using the in-line three-axis AF demagnetizer in parallel with the long-core magnetometer (Fig. 2). The directions of the characteristic remanent magnetization (ChRM) were then determined by principal component analysis (Kirschvink 1980), normally based on AF demagnetization results from 15 to 65 mT. Neither core was obtained with azimuthal orientation, so the mean ChRM declination of the whole core was set to zero. Stacked records of inclination and declination were obtained after development of a depth-age model (see below) by numerical resampling into 0.1 kyr time bins and subsequent calculation of arithmetic mean values. An anhysteretic remanent magnetization (ARM) was produced along the positive z-axis of the samples with 0.05 mT static field and 100 mT AF using a separate 2G Enterprises 600 single-axis AF demagnetizer with an

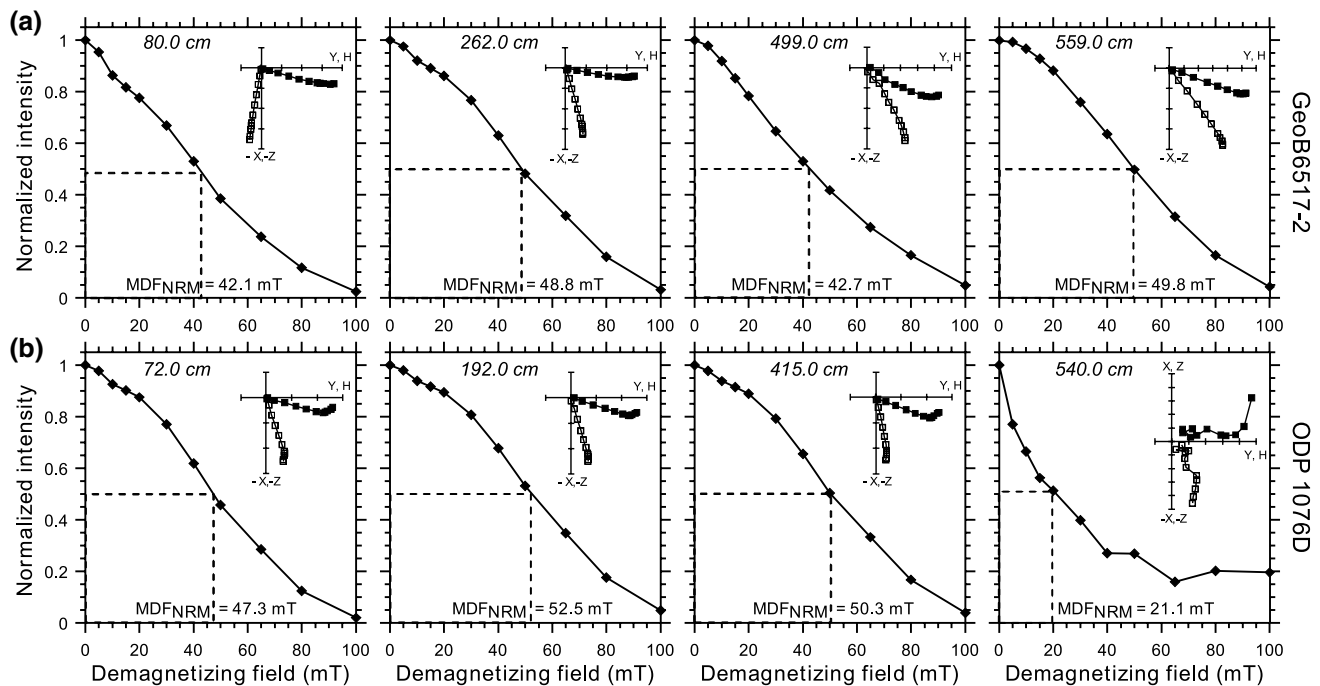


Fig. 2 Alternating field demagnetization results for the natural remanent magnetization (NRM) of four samples each from **a** core GeoB6517-2 and **b** core ODP 1076D. Sampling depth refers to the individual core depth. Embedded plots indicate the corresponding orthogonal projections (vector endpoint diagrams) of components

during stepwise demagnetization. Demagnetization steps run from 0 to 100 mT. Closed symbols denote X (north) plotted versus Y (east) in the horizontal plane (declination changes), and open symbols denote Z (vertical) plotted versus H (horizontal)

ARM-coil. The ARM intensities (J_{ARM}) were then measured and demagnetized with the 2G Enterprises 755 SRM at the same levels as the NRM.

A saturation isothermal remanent magnetization (SIRM) was imparted in a 1.5 T field with a 2G Enterprises 660 pulse magnetizer along the sample's positive z -axis and was measured with a Molyneux MiniSpin flux-gate magnetometer. S-ratios with a backfield of -0.2 T were calculated as $0.5 \times (1 - (\text{IRM}_{-0.2\text{T}}/\text{SIRM}_{1.5\text{T}}))$ following Bloemendal et al. (1992). The ARM mainly represents fine-grained magnetic particles (mainly magnetite). Its intensity normalized by the amplitude of the static field used for imparting the ARM is defined as the anhysteretic susceptibility κ_{ARM} . The low-field magnetic susceptibility κ_{LF} and the SIRM represent the whole magnetic fraction, so both $\kappa_{\text{ARM}}/\kappa_{\text{LF}}$ and $J_{\text{ARM}}/J_{\text{SIRM}}$ (J for intensity) can be used as proxies for the presence of fine magnetic particles.

On a subset of samples, the hysteresis parameters M_{S} , M_{RS} , B_{C} , and B_{CR} , FORC diagrams, and IRM-acquisition curves were measured, each at maximum fields of 0.5, 1, and 2 T, with a Princeton Measurements Corporation alternating gradient magnetometer (MicroMag). High-temperature magnetic susceptibility measurements up to

700 °C in an argon atmosphere were performed on three samples from each core with the MFK-1A.

Magnetic extracts were prepared for scanning electron microscope (SEM) analysis following the procedure of Nowaczyk (2011) for one sample from core ODP 1076D and two samples from core GeoB6517-2. Analyses were performed with a Carl Zeiss SMT Ultra 55 Plus SEM with integrated energy-dispersive X-ray spectrometry (EDS), which has a spatial resolution of 1 nm at 15 keV. SEM samples were sputtered with carbon. For imaging in the backscatter high-current mode and for parallel EDS analyses, a working distance of 12 to 13 mm, an aperture of 120 μm , and a voltage of 20 keV were generally used.

Depth-age models and correlation

Depth-age models for cores GeoB6517-2 and ODP 1076D are based on 15 calibrated AMS ^{14}C ages obtained from core GeoB6518-1 (Scheffuß et al. 2005, 2016) (Fig. 3b). To transfer these ages to the two cores investigated, inter-site correlation was performed, based on magnetic susceptibility logs for all three sites (Fig. 3a). Shipboard magnetic susceptibility measurements of ODP 1076D were corrected by a calibration factor of 6.8, as suggested by Blum

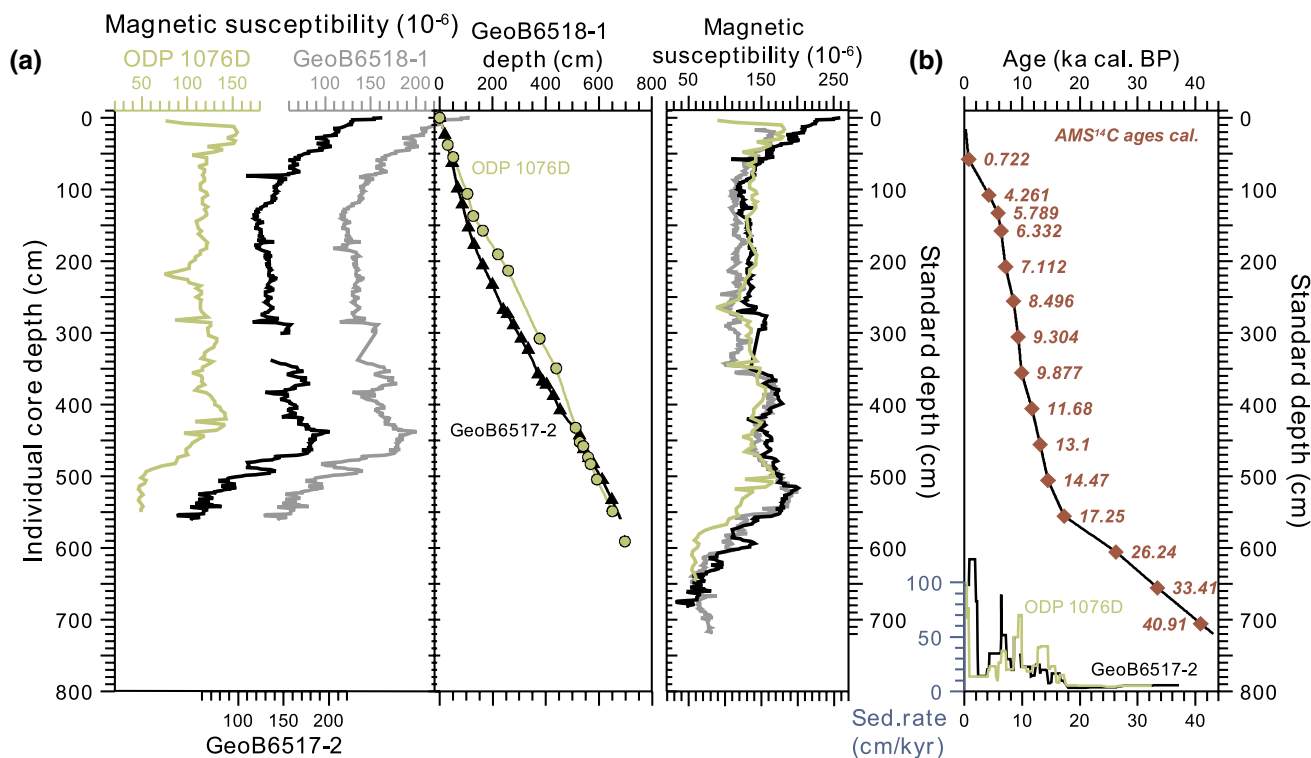


Fig. 3 **a** Inter-core correlation (right) by depth tie-points (middle) between cores GeoB6518-1, GeoB6517-2 and ODP 1076D based on magnetic susceptibility data from the split cores in 1 and 2 cm stratigraphic increments (left), respectively. ODP 1076D data are from the

Ocean Drilling Program (ODP) database, as published by Wefer et al. (1998b). **b** Depth-age model for the studied cores from the Congo Fan and sedimentation rates for cores GeoB6517-2 and ODP 1076D

(1997). Additional information for correlation between cores GeoB6518-1 and GeoB6517-2 was obtained from the records of pore water content and density (Müller 2003a, b), as well as unpublished geochemical data sets (Müller 2004a, b). The correlation between cores GeoB6517-2 and ODP 1076D is supported by rock magnetic results. The uncorrelated and correlated susceptibility records are shown in Fig. 3a along with the correlation models. In the following, palaeo- and rock magnetic results are presented either on a standard depth-scale, identical to the depth in core GeoB6518-1, or versus age.

Results and discussion

Characterization of the magnetic mineralogy

Depth profiles of rock magnetic parameters for GeoB6518-2 and ODP 1076D are presented in Fig. 4 versus standard depth to point out the main similarities and differences between the two cores. Above 380 cm, all parameter variations are mostly similar with smaller differences in magnetic mineral concentration toward the top of the cores as visible

in J_{ARM} and J_{SIRM} . Below 380 cm, these differences are more prominent, with two intervals of distinctly higher magnetic mineral concentration in core GeoB6517-2 and a slightly higher fine-grained ferrimagnetic particle content in ODP 1076D between 450 and 520 cm (Fig. 4), as reflected by higher $\kappa_{\text{ARM}}/\kappa_{\text{LF}}$ values. The depth range between 380 and 520 cm includes the Holocene/Pleistocene boundary. Sea-level rise after the end of the last glacial period resulted in a more homogeneously distributed sediment load from the Congo River to the Northern Congo Fan. Below 570 cm, the decreased magnetic mineral concentration in both cores is the most obvious indicator that the magnetic fractions in both cores are affected by reductive diagenesis.

High-temperature magnetic susceptibility measurements indicate that there is a complex mixture of Fe-bearing minerals within the sediments (Fig. 5a). The sediments contain Fe-sulfides and different clay minerals (Wefer et al. 1998b; Spieß and Cruise 2002). Studies on the sediment load of the Congo River indicate that up to 10% of the suspended load consists of iron oxyhydroxides due to the predominance of chemical erosion in the catchment area (Eisma et al. 1978), which has led to ferrosol formation (Collins et al. 2010). Hematite and hematite-coated quartz grains, which probably

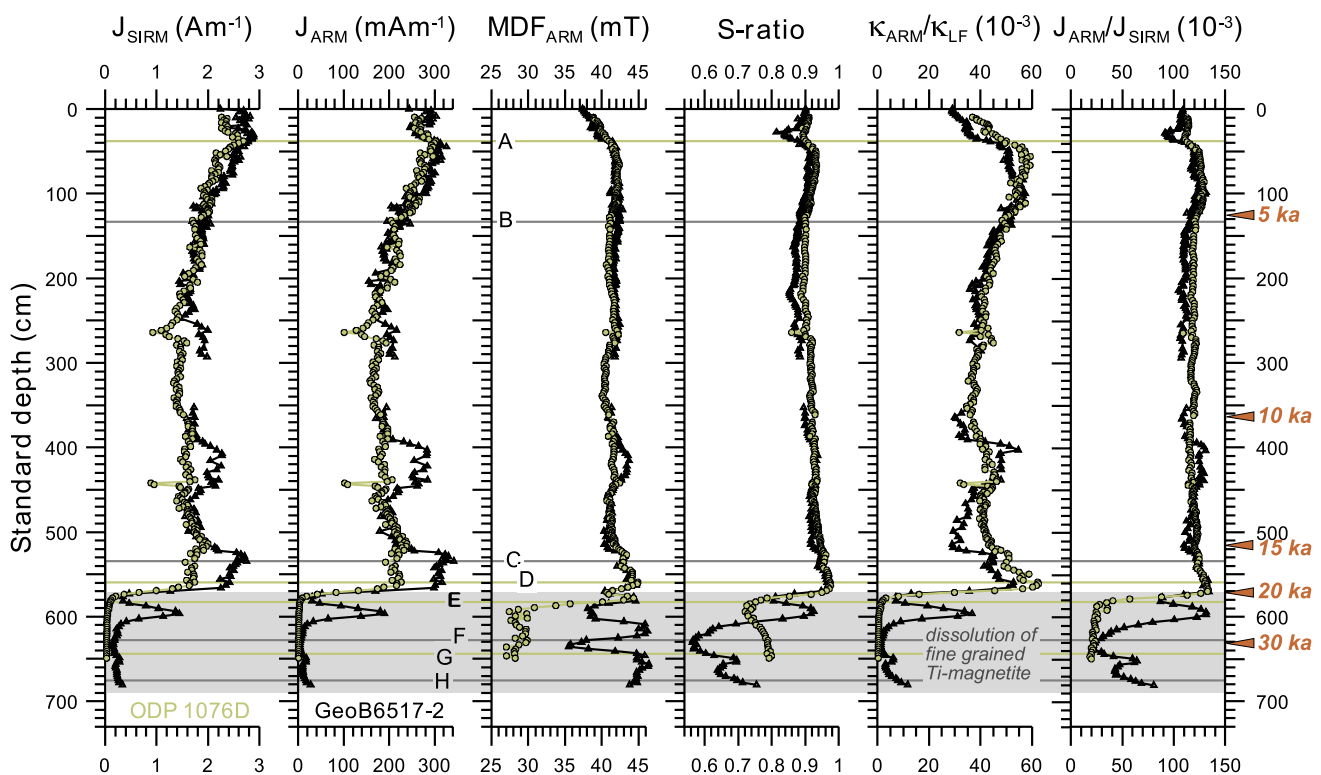


Fig. 4 Rock magnetic parameters for cores GeoB6517-2 (black) and ODP 1076D (green) versus standard depth as defined in Fig. 2. From left to right: intensities of the saturation isothermal remanent magnetization (J_{SIRM}) and anhysteretic remanent magnetization (J_{ARM}), median destructive field of the ARM (MDF_{ARM}), S-ratio, $\kappa_{\text{ARM}}/\kappa_{\text{LF}}$

and $J_{\text{ARM}}/J_{\text{SIRM}}$. The horizontal lines and capital letters denote the positions of samples shown in Figs. 5, 7, 9, and 14. Black lines: core GeoB6517-2; green lines: ODP 1076D. Age-scale indicators are given by the red arrows and numbers to the right

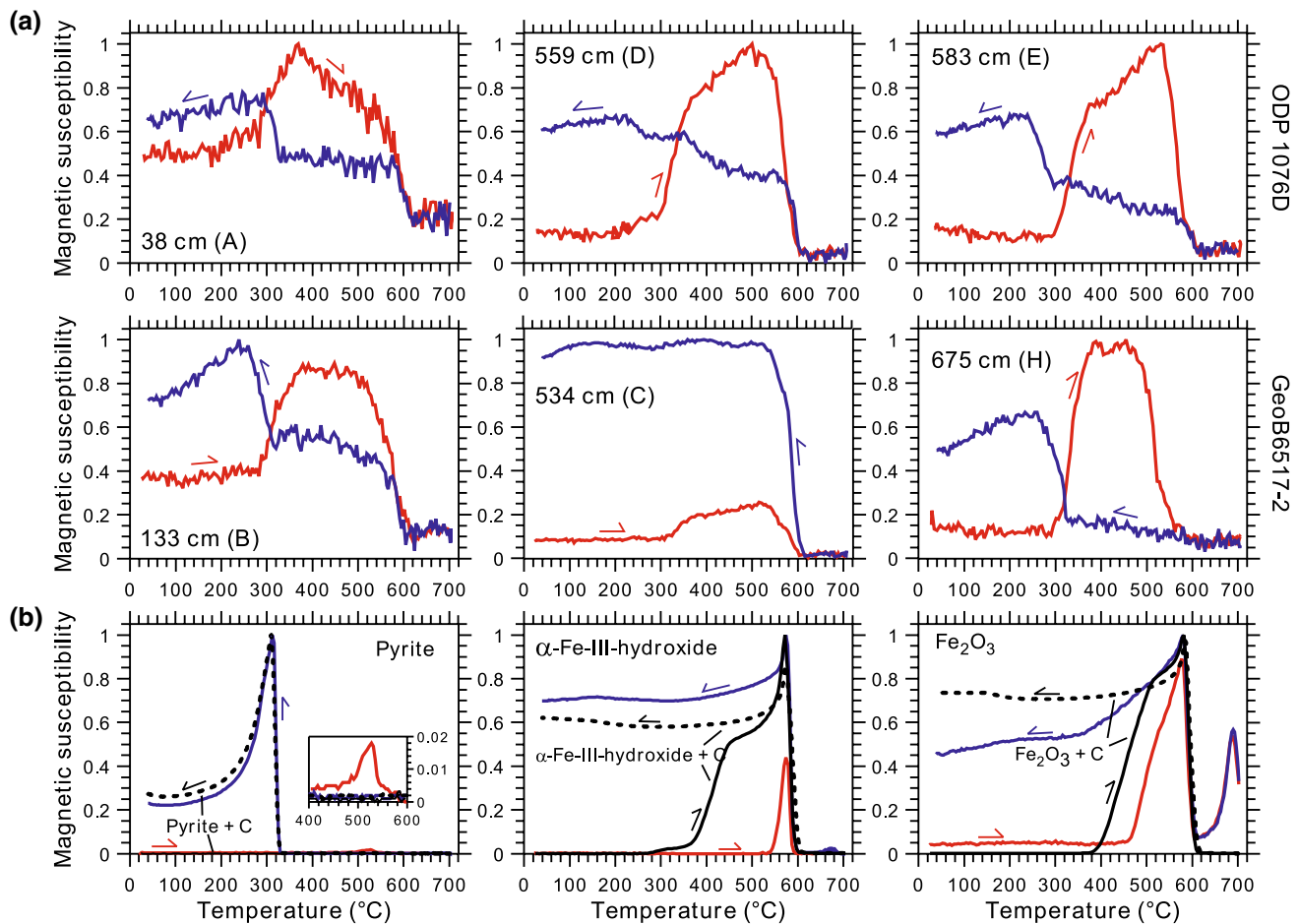


Fig. 5 High-temperature magnetic susceptibility measurements for **a** six representative sediment samples and **b** a set of artificially mixed samples. The capital letters refer to Fig. 4 where the stratigraphic positions of the samples are marked by horizontal lines. The iron-bearing minerals used for comparison are those assumed to

be present in the sediment. They were mixed with aluminium oxide and activated carbon. See text for details. Red denotes heating, blue denotes cooling curves, and solid and dashed black curves represent results from synthetic samples with and without additional carbon, respectively. All samples were measured in an argon atmosphere

originate from red sandstones in the lower Congo region, were identified by heavy-mineral separation for sediment recovered in cores from the Congo canyon to the south (Heezen et al. 1964).

To identify individual components in the high-temperature curves, natural pyrite, synthetic α -Fe-III-hydroxide (Alfa Aesar[®] GmbH & Co KG, Karlsruhe, Germany), and synthetic Fe_2O_3 (for technical characteristics see Frank and Nowaczyk 2008) were mixed separately with (a) Al_2O_3 and (b) Al_2O_3 plus 8 wt% activated charcoal. These mixtures were then measured under the same conditions as the sediment samples (Fig. 5b). In the artificial samples, the charcoal represents the organic carbon content in the natural sediments. This is relevant, because experiments on a variety of iron-bearing minerals commonly found in soils have shown that at least high-temperature measurements in air are strongly influenced by the presence of carbon (Hanesch et al. 2006; Minyuk et al. 2011). There is generally little

difference between the cooling curves of synthetic samples with and without C (Fig. 5b). However, heating curves for α -Fe-III-hydroxide and Fe_3O_4 with and without C are different, with a much earlier onset of magnetite/maghemite formation when carbon is present, and more pronounced transformation steps, which resemble strongly the heating curves obtained from the natural sediment samples (Fig. 5a). In addition, hematite is reduced to magnetite/maghemite in the presence of C (Hanesch et al. 2006; Minyuk et al. 2011) and is visible neither in heating nor cooling curves for synthetic samples. In sediment samples where intergrowth of magnetic minerals with host rock minerals is to be expected, hematite is visible to some degree in some heating and cooling curves above 580 °C (Fig. 5a). Pyrite (FeS_2), due to baking out of sulfur, transforms into pyrrhotite (Fe_7S_8) during heating with Curie temperature of ~ 325 °C (Dekkers 1989), but there is no formation of magnetite from pyrite with carbon present (Fig. 5b). The observed formation of

magnetite and most likely maghemite in all sediment samples starting at around 300 °C (Fig. 5a) is, therefore, not caused by alteration of pyrite (e.g., Passier et al. 2001), but is presumably due to the presence of either Fe-bearing paramagnetic minerals like smectite, illite, or biotite (Ellwood et al. 2007; Minyuk et al. 2011; Hirt et al. 1993) or, more likely, Fe-hydroxides and hematite, as shown by our experiments on pure minerals (Fig. 5b). The characteristic fingerprint for the presence of pyrite in the studied sediments is the distinct susceptibility increase in cooling curves below 325 °C (Fig. 5a) related to the Hopkinson peak of newly formed ferrimagnetic pyrrhotite (Dekkers 1989). Although (Ti-)magnetite is not properly visible in high-temperature curves, it was identified in SEM images of magnetic extracts from both cores together with pyrite (Fig. 6a, b), and rutile as an accessory mineral (Fig. 6c).

IRM acquisition curve analysis with IRMUNMIX (Heslop et al. 2002) reveals that the magnetic fraction contains up to three ferrimagnetic components distinguished by their different grain sizes and by one high-coercivity component, most likely hematite (Fig. 7). Goethite will mainly be evident in fields below 2 T (Rochette and Fillion 1989; Rochette et al. 2005). A scatter plot of the dispersion parameter (DP) versus $B_{1/2}$ for all measured samples indicates a clear clustering of the single components and grain-size fractions (Fig. 8) with no obvious difference between results from both cores. The ultra-fine-grained ferrimagnetic component (black) has a mean $\log B_{1/2}$ of 1.7 mT and a dispersion < 0.2 (Fig. 8),

which corresponds to the values obtained for biogenic magnetite (Egli 2004; Roberts et al. 2012). The latter is found commonly in a wide range of marine environments, and can be dominant in sediments with high carbonate content (see Roberts et al. 2012 and references therein). Abundant living magnetotactic bacteria were found in the upper cm of hemipelagic sediments along the West African coast (Hilgenfeldt 2000; Petermann and Bleil 1993).

In addition, FORC diagrams for samples A and D (Fig. 9) clearly contain a narrow central ridge that is typical of weakly interacting SD particles (Roberts et al. 2000), as would be expected for isolated intact magnetofossil chains dispersed in the sediment (Egli et al. 2010; Roberts et al. 2012). In contrast, the FORC diagram for sample E from anoxic sediments (Fig. 4) has a mixed assemblage of SD and lower coercivity signatures (Fig. 9) (Roberts et al. 2000), which resemble those recently associated with the vortex state by Roberts et al. (2017). This is consistent with the results of IRM-acquisition analysis (Fig. 7) and the low $J_{\text{ARM}}/J_{\text{SIRM}}$ values (Fig. 4). An aeolian origin for the ultra-fine-grained component as suggested by Bloemendal et al. (1988) for fine-grained material in cores offshore of Senegal is unlikely here. End-member modelling based on the major element composition of dust, suspended river sediment, and marine sediment originating from West Africa indicates that, in sediments from the Congo Fan, the riverine component dominates throughout the whole time interval investigated (Collins et al. 2010). Part of the fine-grained

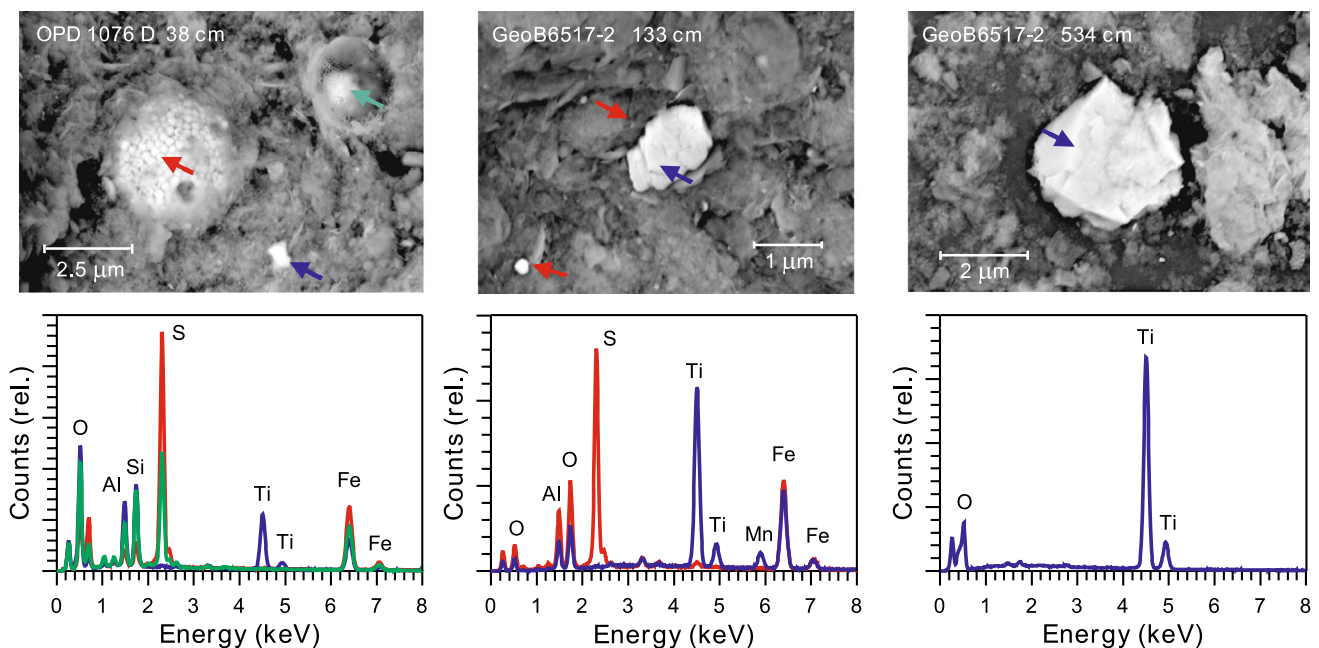


Fig. 6 SEM images of a pyrite framboid and small Ti-magnetites (left, middle) and rutile (right) found in magnetic extracts from cores ODP 1076D and GeoB6517-2. Spots for energy-dispersive X-ray

element analyses, shown below each photo, are indicated with correspondingly coloured arrows

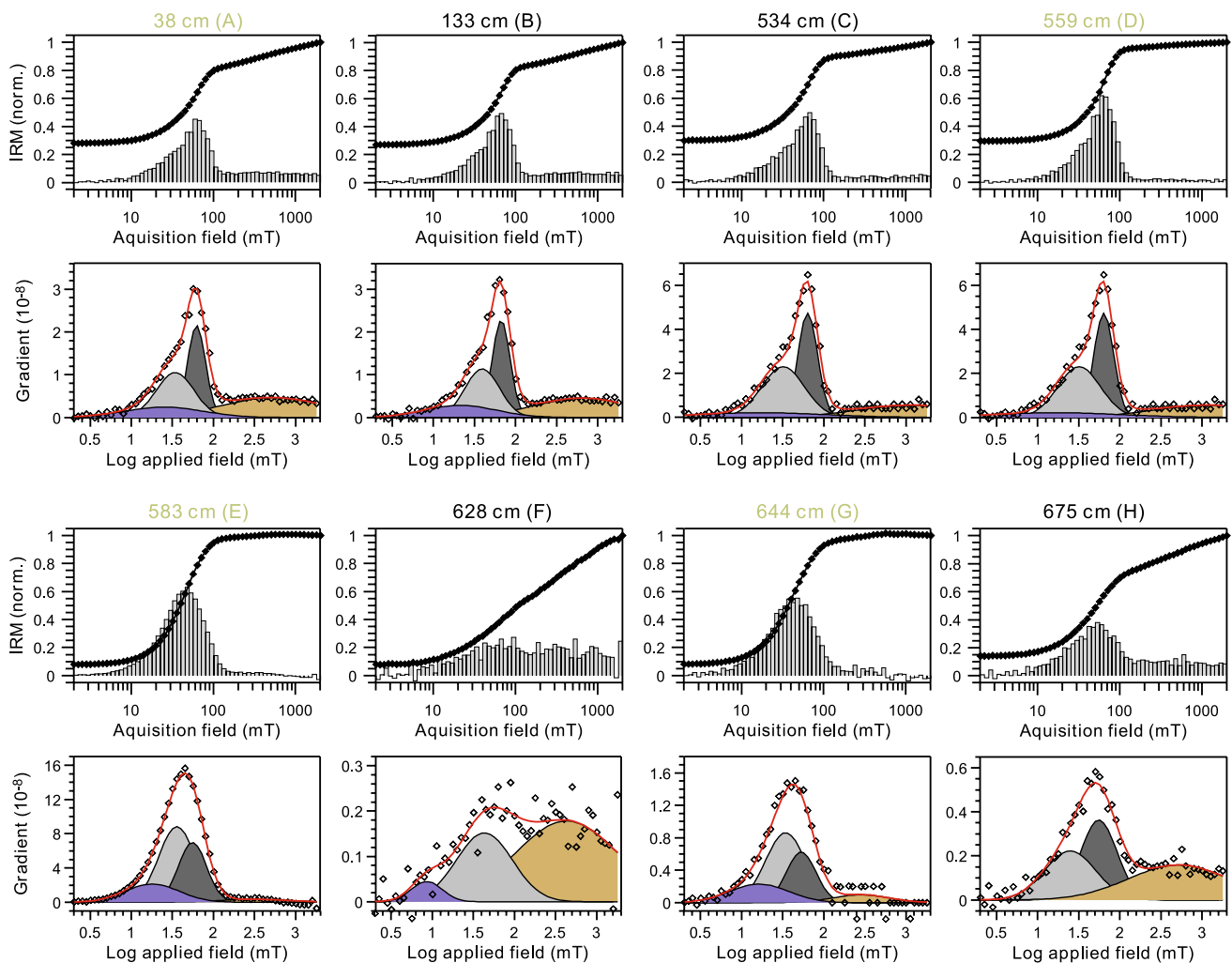


Fig. 7 Acquisition curves of an isothermal remanent magnetization (IRM) (top) and corresponding component analysis results (bottom) for eight samples from cores GeoB6517-2 and ODP 1076D in stratigraphic order. The capital letters (GeoB6517-2: black, ODP 1076D: green) refer to Fig. 4 where the stratigraphic positions of the samples are marked by horizontal lines. Grey bars below the IRM-acquisition

ferrimagnetic fraction is, therefore, probably the product of chemical weathering and soil formation in the Congo basin, which contributes to the mixture of detrital (Ti-)magnetite and biogenic magnetite in the sediments.

The high ultra-fine-grained magnetite content is also visible in Fig. 4, with high $\kappa_{\text{ARM}}/\kappa_{\text{LF}}$ and $J_{\text{ARM}}/J_{\text{SIRM}}$ values corresponding to the values determined for sediment cores from the Guinea Basin (Itambi et al. 2010), the Niger deep-sea fan (Dillon and Bleil 2006), and offshore of Senegal (Bloemendal et al. 1988; Itambi et al. 2009). The dominance of fine-grained (Ti-)magnetite is limited to the sediment above 570 cm depth (Figs. 4, 7 samples A to D). Below 570 cm in both cores, the rock magnetic fraction is heavily altered due to reductive diagenesis, which is a common phenomenon in sediments from along the West African coast and

plots represent the IRM-acquisition rate. Red lines in the component analysis denote the sum of components, and black diamonds represent the raw data. The hematite component is marked by golden colours, whereas other colours represent different ferrimagnetic grain-size fractions with variable coercivities

the South Atlantic Ocean (Wefer et al. 1998a, b; Channell et al. 2000; Stoner et al. 2003; Dillon and Bleil 2006; Itambi et al. 2010). Diagenetic alteration of the magnetic fraction is visible not only as a loss of magnetic mineral concentration (J_{ARM} , J_{SIRM}) but also as an increased mean grain size (low $\kappa_{\text{ARM}}/\kappa_{\text{LF}}$ and $J_{\text{ARM}}/J_{\text{SIRM}}$ values), respectively (Fig. 4). In the sample from 628 cm (F), there is little fine-grained (Ti-) magnetite left, but, instead, the high-coercivity component is dominant (Fig. 7). The observed coercivity decrease in core ODP 1076D, which is expressed by low MDF_{ARM} values below 570 cm, is not in conflict with the increasing dominance of hematite as reflected in the S-ratio (Fig. 4). Studies on artificially mixed hematite and magnetite samples demonstrate that MDF_{ARM} will not increase until the hematite content is higher than 99 wt% of the magnetic fraction,

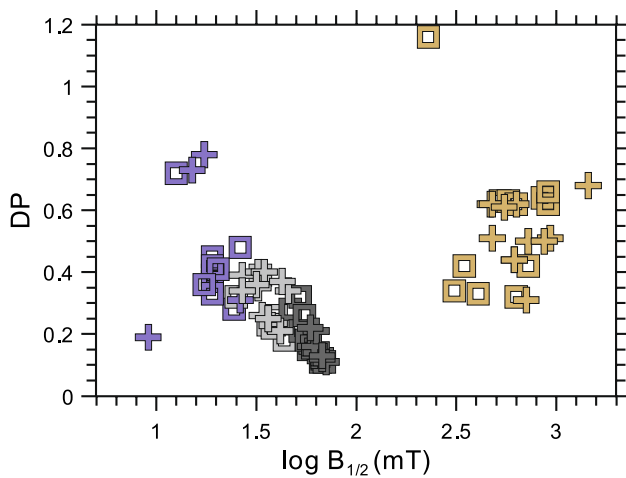


Fig. 8 Scatter plot of $\log B_{1/2}$ and dispersion parameter (DP) values obtained from IRM-component analysis with IRMUNMIX (Heslop et al. 2002) for 24 samples from cores GeoB6517-2 (crosses) and ODP 1076D (open squares). The colour coding is the same as in Fig. 7

which corresponds to an S-ratio of 0.7 (Frank and Nowaczyk 2008). In core GeoB6517-2, this low value is reached, but the MDF_{ARM} is not constantly high (Fig. 4), which indicates that other factors, e.g., grain size, also influence the MDF_{ARM} .

Scatter plots of the main rock magnetic parameters in Fig. 10 highlight the different properties of magnetic fractions from oxic (above 570 cm) and sulphidic sediments (below). They also indicate that the magnetic fraction from core ODP 1076D is more homogeneous, with a lower content of high-coercivity minerals, as visible from the higher S-ratio. Lower magnetic grain-size variability is also reflected by a clustering of J_{ARM}/J_{SIRM} ratios. These differences can be attributed to the distance between the sites and to the position of ODP Site 1076D further to the north of the Congo River mouth compared to GeoB6517-2 (Fig. 1). Although some greigite is evident in the SEM analyses, there is no indication in the magnetic results that greigite makes a major magnetic contribution. None of the representative samples, which are marked by capital letters in Fig. 10, have a combination of high S-ratios and low J_{ARM}/J_{SIRM} values that are typical of greigite (Frank et al. 2007b; Nowaczyk et al. 2012, 2013). We cannot rule out an influence from low concentrations of greigite with thermally relaxed SP and SD properties as reported by Rowan et al. (2009).

Palaeomagnetic directions

ChRM inclination and declination records from both cores are shown in Fig. 11, along with the maximum angular deviation (MAD) and the median destructive field (MDF) of the NRM, which are indicators of the stability of the magnetic

signal during demagnetization. Except for the topmost 40 cm of ODP 1076D, where the sediment was obviously distorted during core recovery, the magnetic signal is stable with MAD values $< 2^\circ$ to a depth of 580 cm (ODP 1076D) and 570 cm (GeoB6517-2), respectively. The low MAD values support the evidence provided above that the magnetic remanence is partly carried by biogenic magnetite. Further down-core, grain-size sensitive parameters point to coarser magnetic mineral grain sizes due to preferential dissolution of the fine-grained (Ti-)magnetite fraction below about 570 cm depth (Fig. 4). The dissolution effect is more pronounced in core ODP 1076D, where the NRM drops to below 1 mAm^{-1} (not shown) and MDF_{NRM} decreases by more than 30 mT below 570 cm (Fig. 11). Inclination and declination variations for core ODP 1076D generally look like geomagnetic palaeosecular variation patterns above 570 cm. The mean inclination is slightly lower than the expected inclination of -10.1° for a geocentric axial dipole field. Below 570 cm, with drastically increased MAD values of $> 15^\circ$, palaeomagnetic directions are scattered.

In core GeoB6517-2, which is located closer to the Congo River mouth, the inclination and declination record is scattered below 350 cm (Fig. 11), which is accompanied by a slight change in sediment composition. This is also documented in colour reflectance profiles and was interpreted to indicate a change in the ratio of oxic versus sulphidic iron contents (Spieß and Cruise 2002). It is not reflected in the MAD or MDF_{NRM} values (Fig. 11). In core ODP 1076D, no such distinct change is visible.

When considered separately, the inclination records from both cores look reasonable. However, when plotted on a common time scale, differences between the signals become obvious. The differences appear as large uncertainties when stacked for comparison with predictions from the existing palaeomagnetic field models (Fig. 12). The inter-site variability also clearly exceeds geomagnetic variation differences expected from such closely adjacent locations. Moreover, comparison with palaeosecular variation curves for the Congo Fan area from the *CALSK10k.2* (Constable et al. 2016) and *pfm9k.1a* (Nilsson et al. 2014) models illustrates differences with respect to the existing field models. Except for the distinct inclination minimum at 9 ka, none of the model features can be clearly identified in either inclination record, although there are some similarities mainly between the GeoB6517-2 record and the models throughout the time interval. There is reasonable to good agreement between the declination records from GeoB6517-2 and ODP 1076D back to about 10 ka, again with GeoB6517-2 having a slight resemblance to the model declination curves (Fig. 12). However, the quality of the sediment signal should not be judged by comparison with the modelled records, because data for low and southern latitudes are sparse, which might result in large uncertainties in the *CALSK10k.2* and *pfm9k.1a*

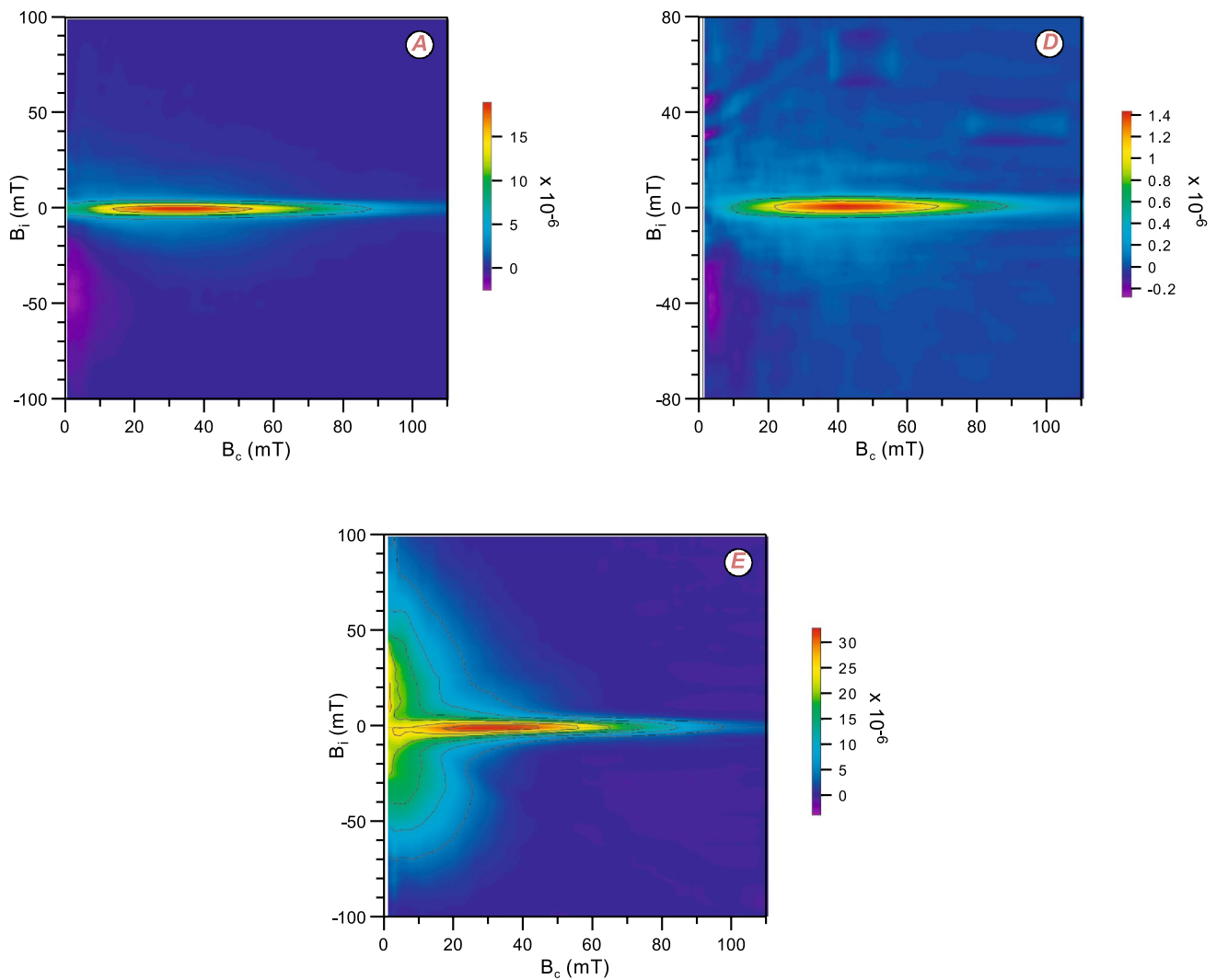


Fig. 9 FORC diagrams for samples from core ODP 1076D. The samples are from depths indicated in Fig. 4: 38 cm (A), 559 cm (D), and 583 cm (E). The FORC diagrams were conventionally measured (150 FORCs were measured with an average time of 100 ms) and pro-

cessed using the VARIFORC protocol (Egli 2013) within the FORCinel software package (Harrison and Feinberg 2008). Note that a smoothing factor (SF) of 5 was adopted for all the samples

models (Constable et al. 2016; Nilsson et al. 2014). This is illustrated clearly by the dispersion between the two model declination curves prior to 6 ka. The new palaeomagnetic records agree most closely for that time interval, which indicates their potential for improving future models for that time interval.

The only published sedimentary PSV records from equatorial West Africa are those from Barombi Mbo, Cameroon (Thouveny and Williamson 1988), which lies about 1100 km north and slightly west of the Congo Fan, and from Lake Bosumtwi, Ghana (Walker 2001), some 2000 km to the northwest (Fig. 1a, c). Both records have outdated chronologies in the original publications, which have been subsequently updated. A new chronology for core BM6 from Barombi Mbo, published by Lebamba

et al. (2012), was applied to the inclination and declination records from Core BM6, which was digitized from Fig. 3 of Thouveny and Williamson (1988). The same depth-age model was also used to date core BM2 separately, because descriptions of the coring sites, NRM records, and radiocarbon ages available for BM2 (Thouveny and Williamson 1988) suggest that the 5 m BM2 core corresponds to the topmost 4.5 m of BM6 rather than to the interval between 4 and 7 m as originally published. The individual records for both cores are shown in Fig. 13a, b. Differences in the timing of PSV features caused by this update are illustrated in supplemental Fig. S1 by comparison of the records both plotted on the old and new age scales. For Lake Bosumtwi, the NRM data after demagnetization at 50 mT were digitized from Fig. 13 of Walker (2001)

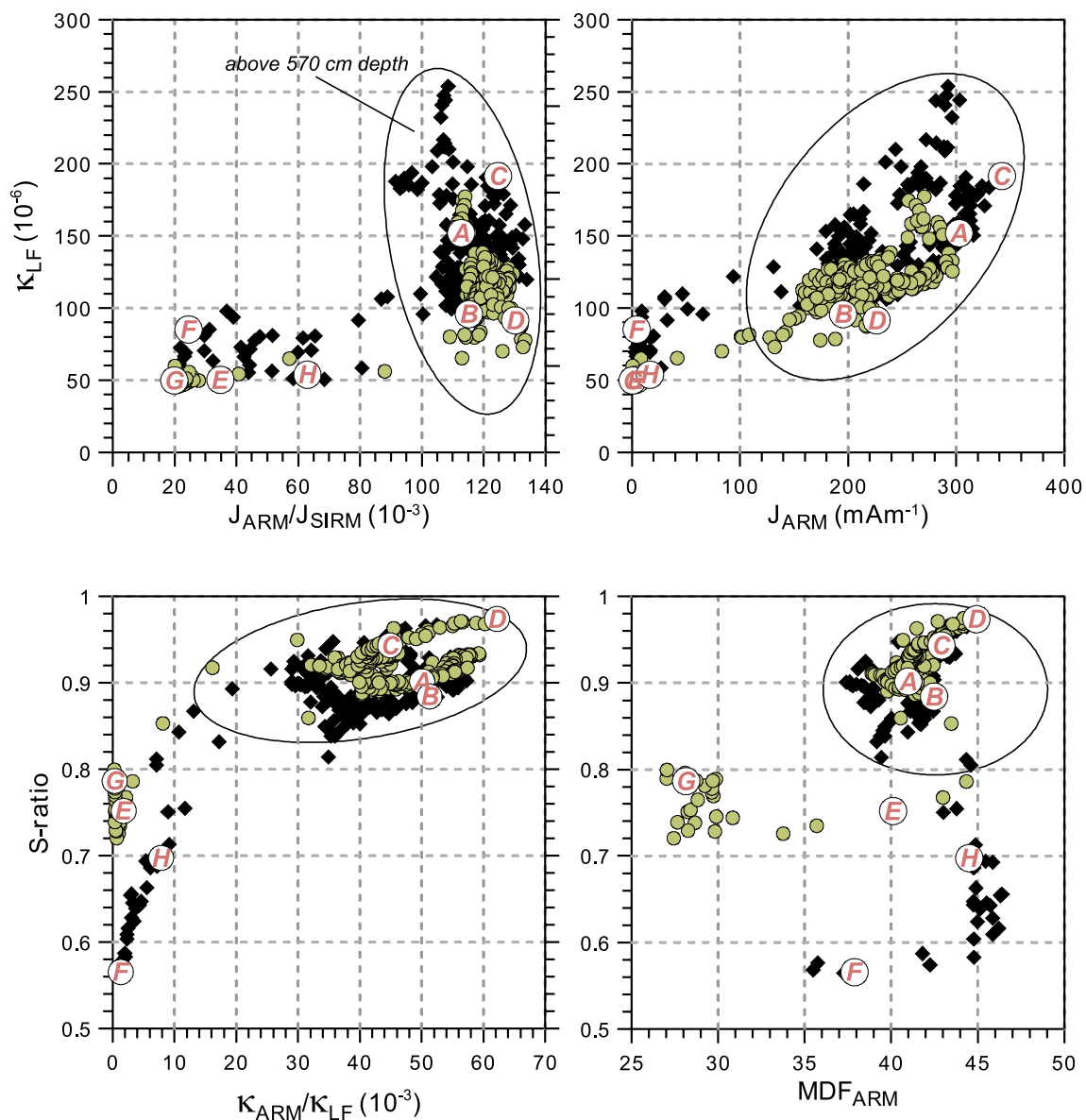


Fig. 10 Scatter plots of the main measured magnetic parameters, which highlight the differences between the magnetic fractions from Core GeoB6517-2 (black diamonds) and Core ODP 1076D (green filled circles). The capital letters refer to Fig. 4 where the stratigraphic

positions of the samples are marked by horizontal lines. Data that plot within the areas marked by ellipses (including A to D) are from oxic sediments (above 570 cm depth) and others (including E to H) are from anoxic sediments (below 570 cm depth)

and were then dated with the depth-age model of Shanahan et al. (2012). Additionally shown in Fig. 13a, b are the records of core MAL98-3P from Lake Malawi (Lund et al. 2016), which is situated only ~500 km to the south, but some 2500 km to the east (Fig. 1c). Given the large distances between available records, we must consider how close a correlation can be expected. Comparison of model curves for all the locations in supplemental Fig. S2 suggests that both inclination and declination correlations between the new Congo Fan, the Lake Barombi Mbo, and Lake Bosumtwi records should be high, while differences

to the Lake Malawi record, in particular declination, might also be due to spatial geomagnetic field variability.

In general, the amplitudes of the marine PSV records are lower than those of the lacustrine records (Fig. 13). This is probably due to the lower sedimentation rates of cores GeoB6517-2 and ODP 1076D when compared with Barombi Mbo (Lebamba et al. 2012) and Lake Bosumtwi (Walker 2001; Shanahan et al. 2012). In addition, more intense bioturbation might contribute to the low amplitudes of the marine records by leading to averaging over a larger depth interval and thus damping short-frequency variations.

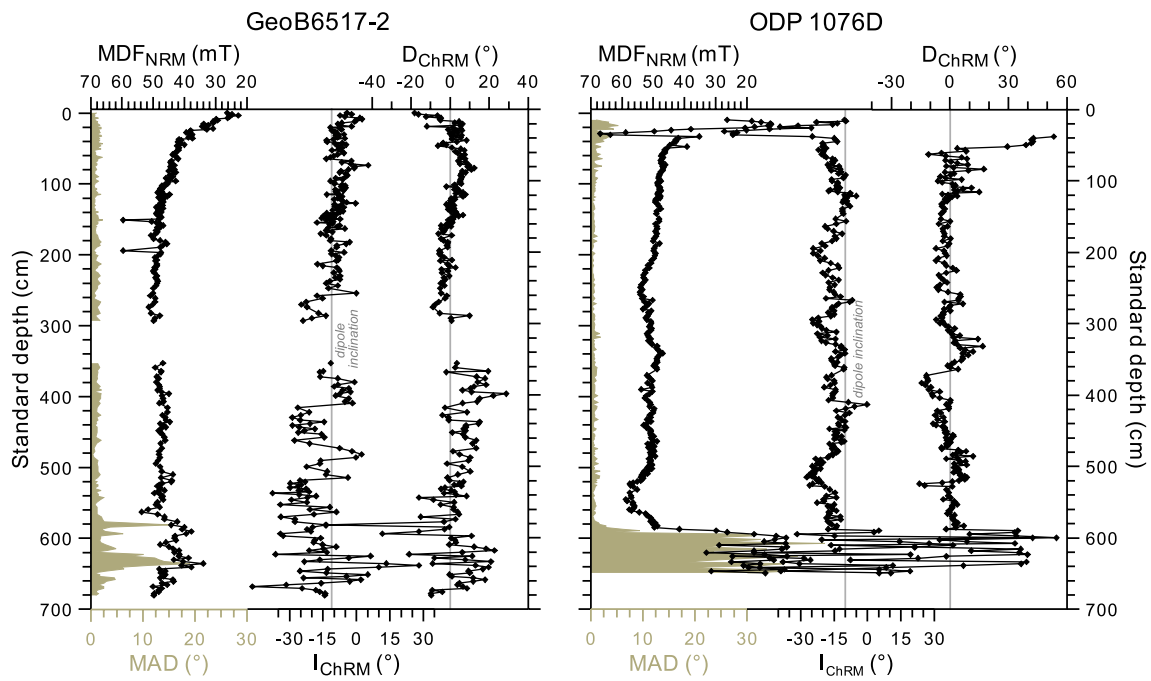


Fig. 11 Palaeomagnetic directions for the ChRM inclination (I_{ChRM}) and declination (D_{ChRM}) records for cores GeoB6517-2 (left) and ODP 1076D (right) with the respective median destructive field

(MDF_{NRM}) and maximum angular deviation (MAD) records. All curves are plotted versus standard depth

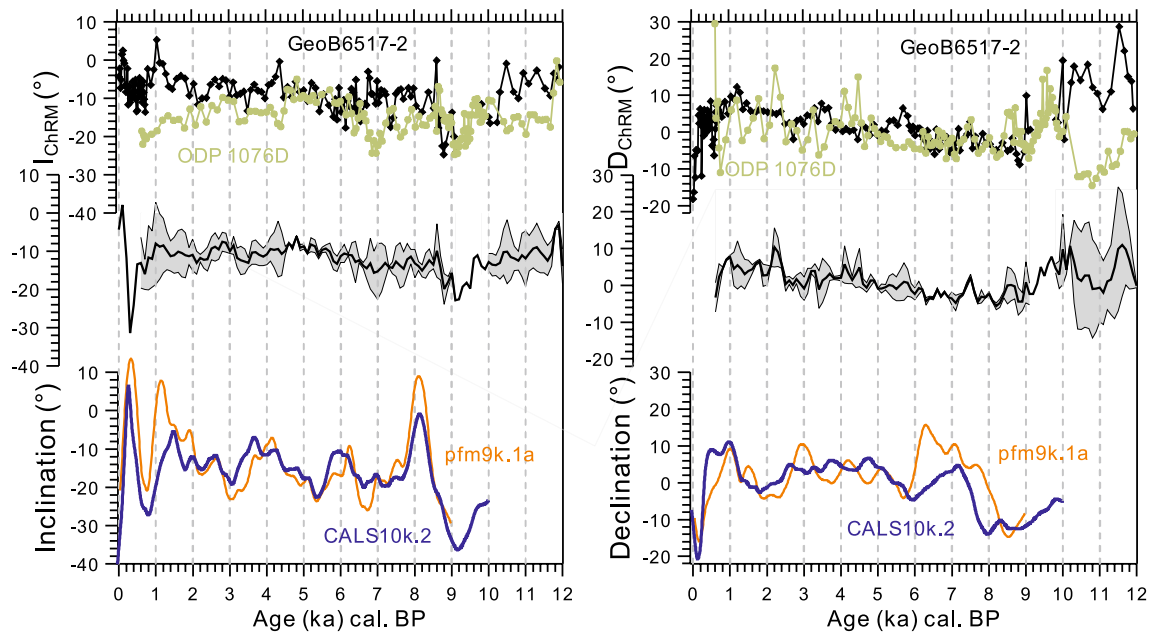
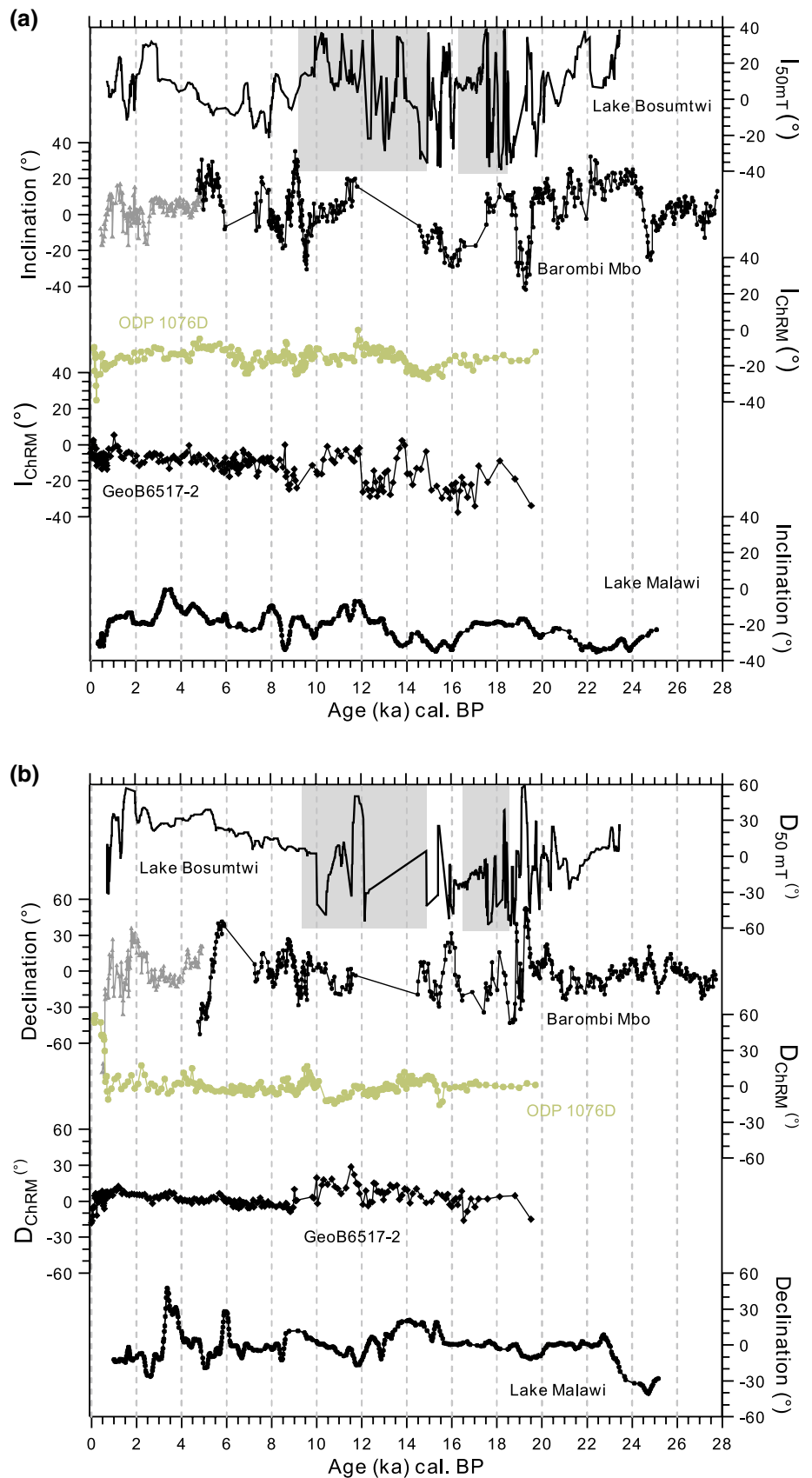


Fig. 12 Comparison of the I_{ChRM} and D_{ChRM} records for cores GeoB6517-2 (black) and ODP 1076D (green) with model results from CALS10k.2 (Constable et al. 2016) and pfm9k.1a (Nilsson et al. 2014) for the study area

Despite the fact that the inclination records in Fig. 13a appear to be different at the first sight, several variations are coherent in their general trends, although not in amplitudes,

and have slight offsets in time, which is not uncommon for independently dated records. The records from the Congo Fan, Lake Barombi Mbo, and Lake Malawi have more or

Fig. 13 Compilation of inclination (a) and declination records (b) from low-latitude Africa: Lake Bosumtwi (Walker 2001), Barombi Mbo (Thouveny and Williamson 1988), cores ODP 1076D and GeoB6517-2 (this study), and Lake Malawi (Lund et al. 2016). Data for Barombi Mbo, Lake Bosumtwi, and Lake Malawi were digitized from the respective publications and age models for the first two records were updated here. For more details, see text. Grey-shaded areas in the Lake Bosumtwi records mark intervals with low magnetic intensity and magnetic mineral concentration (Walker 2001)



less pronounced inclination minima at around 1, 7, 9, and 14 to 16 ka, a broad maximum between 4 and 6 ka, and a sharp maximum at about 9 ka. Except for GeoB6517-2, a decreased inclination can be observed over about two millennia between 12 and 14 ka. These features appear to be clearer in ODP 1076D than in GeoB6517-2, which, as mentioned earlier, probably does not reflect geomagnetic variations below 350 cm (prior to approximately 9 ka). Several of these features also appear in the Bosumtwi record, although it is an inclination record based on blanket demagnetization at 50 mT (Walker 2001) rather than a ChRM. Available rock magnetic data, however, indicate that the magnetic mineral fraction in the Bosumtwi sediments is fairly homogeneous with regard to grain size, coercivity, and mineralogy over the last 10 kyr (Peck et al. 2004; Walker 2001). Thus, recorded variations for this time interval are considered to reflect true geomagnetic field variations.

There are fewer similarities for the declination records between the five curves presented (Fig. 13b), although they have some common features like a maximum (easterly declination) between 8 and 10 ka that is visible at ODP 1076D, Lake Barombi Mbo, and the more distant Lake Malawi or a minimum (westerly declination) at around 15 ka. Further processing of the inclination and declination records of cores ODP 1076D and GeoB6517-2 as a step toward developing a master curve for equatorial West Africa is on hold until results from ongoing investigations on new drill cores from Barombi Mbo taken in 2015 become available.

Estimation of relative palaeointensity

We attempt to reconstruct relative palaeointensity (RPI) variations through suitable NRM normalization to account for the observed variations in magnetic mineral concentration, grain size, and coercivity. The NRM after demagnetization at 20 mT ($J_{\text{NRM}20}$) was divided by either κ_{LF} , J_{SIRM} , or ARM after 20 mT demagnetization ($J_{\text{ARM}20}$), and the records were then normalized to their respective mean values. The results, along with normalization parameters and $\kappa_{\text{ARM}}/\kappa_{\text{LF}}$, as an indicator of magnetic mineral grain size, are shown in Fig. 14a, b.

As can be seen in scatter plots of the estimated RPI, calculated with κ_{LF} , J_{SIRM} , and $J_{\text{ARM}20}$, plotted versus $\kappa_{\text{ARM}}/\kappa_{\text{LF}}$, there is no obvious correlation between grain size and the RPI estimates for core GeoB6517-2 (Fig. 14a), but there is possibly for ODP 1076 (Fig. 14b), at least for the $J_{\text{ARM}20}$ or J_{SIRM} normalizers. Here, samples with lower intensities are apparently linked to finer magnetic grain sizes, which is opposite to what would be expected regarding the composition of the magnetic fraction. This misinterpretation is generated by the presence of two main groups of samples with the normalized RPI values > 1 and those with values < 1 (Fig. 14b). A third group with RPI values below 0.5 belongs

to the samples from the topmost 40 cm of the core. Within these groups, there is a little variation in RPI values and no linear correlation with grain size (Fig. 14b). Nevertheless, data from both cores should be treated with caution, especially because the magnetic fraction most likely contains biogenic magnetite and detrital (Ti-)magnetite.

RPI records can be evaluated by comparison to absolute palaeointensity data in addition to the consideration of rock magnetic criteria (King et al. 1983; Tauxe 1993). No absolute palaeointensity data are available from equatorial Africa, so we first compare the data to intensity values given by the *CALS10k.2* (Constable et al. 2016) and *pfm9k.1a* (Nilsson et al. 2014) models. As can be seen in Fig. 15, there is a little similarity between the modelled curves and the estimated RPI records from cores GeoB6517-2 and ODP 1076D except for the last 4 kyr. This, in itself, does not preclude the reliability of our data, because the validity of models for this region is limited or questionable because of a lack of data. More problematic is the fact that the $J_{\text{NRM}20}/J_{\text{ARM}20}$ records from both cores are less similar than expected from comparison of rock magnetic parameters (Fig. 4). The RPI curve from core ODP 1076D decreases since 12 ka with little variations, whereas the record from core GeoB6517-2 has higher variability with an increase between 12 and 9 ka and a decrease during the last 5 kyr (Fig. 15). This difference is probably caused by differences in depositional environments, which leads to higher amounts of detrital (Ti-) magnetite and hematite in core GeoB6517-2, as can be seen in κ_{LF} , J_{ARM} , and the S-ratio (Fig. 10). The latter is more sensitive to high-coercivity minerals than MDF_{ARM} , which is nearly identical in both cores (Figs. 4, 10). This result also indicates that the estimated RPI record is affected by the composition of the magnetic mineral fraction.

The closest RPI record to the Congo Fan is from Lake Malawi (Lund et al. 2016), about 2600 km away (Fig. 1c). Although even more distant, a low-latitude Caribbean record (Frank et al. 2017), more than 8000 km distant, and the South Atlantic Palaeointensity Stack (SAPIS) (Stoner et al. 2002), about 4000 km away, are included in the comparison (Fig. 16, see Fig. 1c for locations). The complete NRM20/IRM20 record from Lake Malawi core MAL98-3, superimposed upon the NRM10/IRM10 and NRM40/IRM40 records in Fig. 10 of Lund et al. (2016), was digitized and the published age model was applied. Although Lund et al. (2016) stated that high RPI values between 6 and 11 ka are probably an artefact caused by normalization with low SIRM20 values; they are shown here for comparison with regard to the influence of depositional environment changes. Moreover, we probably should not expect close correlations between African data and the Caribbean record, because the comparison of model predictions for these locations (supplemental Fig. S2) suggests that the large separation may allow notable centennial to millennial scale variation differences.

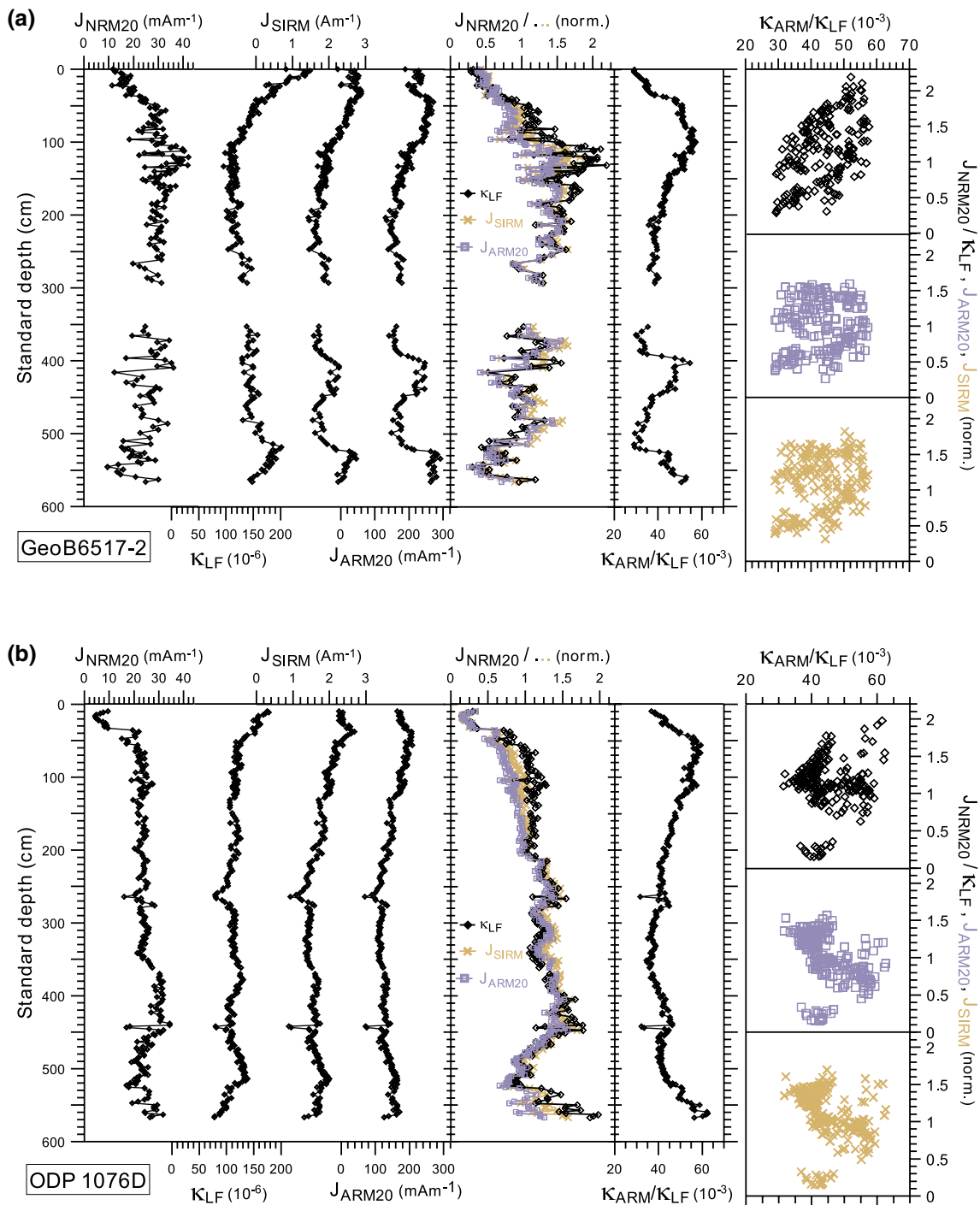


Fig. 14 From left to right, down-core logs of NRM intensity after AF demagnetization at 20 mT (J_{NRM20}), of concentration-dependent parameters κ_{LF} , J_{SIRM} , and J_{ARM20} used as RPI normalizers ($=J_{NRM20}$ divided by κ_{LF} , J_{SIRM} , and J_{ARM20}), and of the grain-size-dependent

parameter κ_{ARM}/κ_{LF} for cores: **a** GeoB6517-2 and **b** ODP 1076D. Right-hand side: scatter plots of the estimated RPI (calculated with κ_{LF} , J_{SIRM} , and J_{ARM20}) versus κ_{ARM}/κ_{LF}

Comparison between the records in Fig. 16 indicates little similarity. The closest agreement surprisingly occurs between the distant records from ODP 1076D and the Caribbean during the past 10 ka, while there is no obvious

correlation between the two neighbouring Congo Fan sites except for a strong decrease during the youngest time interval. Comparing Lake Malawi to SAPIS, it is questionable whether the youngest part of the record gives a

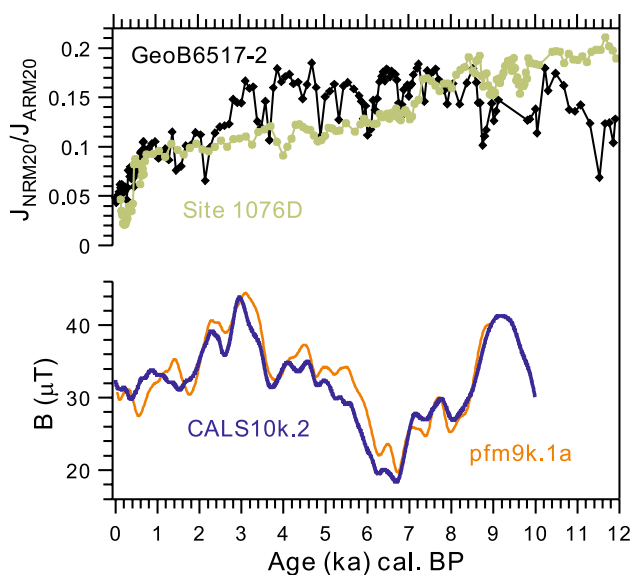


Fig. 15 Comparison of the J_{NRM20}/J_{ARM20} records for cores GeoB6517-2 and ODP 1076D over the time interval from 0 to 12 ka, with the field intensity (B) as predicted by the *CALS10k.2* (Constable et al. 2016) and *pfm9k.1a* (Nilsson et al. 2014) models for the study area

more reliable representation of RPI than the problematic interval between 11 and 6 ka that is affected by sediment composition (Lund et al. 2016). The more critical point in this record is the transition from the late Glacial into the Holocene (13 to 11 ka), which is characterized by a steep $NRM20/SIRM20$ increase (Fig. 16) caused by a distinct magnetic grain-size change (Lund et al. 2016). In records from core GeoB6517-2 and the Caribbean, this transition is visible as an intensity minimum, an artefact caused by magnetic grain-size variations (Fig. 14b, Frank et al. 2017). Several climatic factors that control sedimentation in marine and lacustrine environments underwent pronounced changes during the transition from the Pleistocene to the Holocene. For the studied site, close to the Congo River mouth for example, increased global sea level resulted in changes in coastal current systems and changes in precipitation patterns that led to changes in the amount of riverine discharge, thus controlling the overall sediment load composition, the deposition mechanism, and redox conditions at the water/sediment interface and below (Dupont 2008; Marret et al. 2008; Weijers et al. 2009). Most of the sedimentary RPI records available for this time interval are, in some way, affected by these factors, which often results in thorough modification of the magnetic mineral assemblage, such as in sediments from Lake Malawi, Africa (Lund et al. 2016) (Fig. 16), Lake Lama, northern central Siberia (Frank et al. 2002a, b), the Blake/Bahama Outer Ridge, North Atlantic (Schwartz

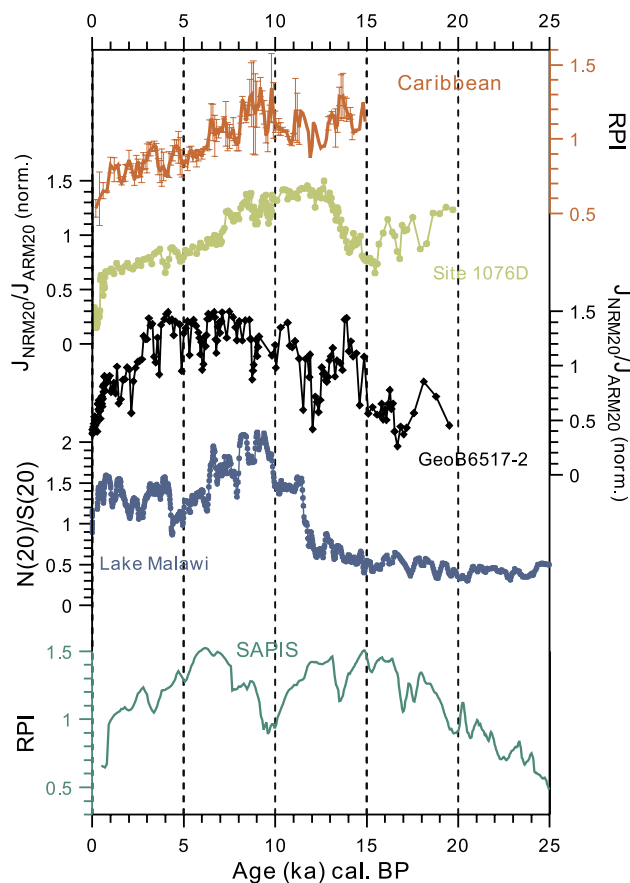


Fig. 16 RPI records from low-latitude areas, the Caribbean Sea (Frank et al. 2017), cores GeoB6517-2 and ODP 1076D (this study), and Lake Malawi (Lund et al. 2016), compared to the South Atlantic Paleointensity Stack (SAPIS) (Stoner et al. 2002)

et al. 1997), or the Black Sea (Nowaczyk et al. 2012, 2013).

The normalization method used in this study is based on the assumption that there is a linear relationship between NRM intensity and geomagnetic field strength during deposition, an assumption which was until recently thought to be valid only for particles in the 1 to 15 μm size (King et al. 1983; Tauxe 1993; Roberts et al. 2012). In sediments from the Upper Congo Fan, there are at least two different ferromagnetic grain-size fractions present, one of which is in the SD range (Fig. 9). Various studies have demonstrated that there is a linear relationship between NRM and applied field for biogenic magnetite carrying a DRM, or pDRM, but with a two-to-four times higher remanence acquisition efficiency compared to detrital (Ti-)magnetite (Pateron et al. 2013; Ouyang et al. 2014; Chen et al. 2017). No time lag was observed between the records carried by biogenic or detrital magnetites in these studies. Transferring these results to the Congo Fan, it must be assumed that the recorded NRM intensity consists of two overlapping signals

acquired at the same time. Based on the extremely high $\kappa_{\text{ARM}}/\kappa_{\text{LF}}$ and $J_{\text{ARM}}/J_{\text{SIRM}}$ values (Fig. 4), and the low MAD values (Fig. 11) obtained for cores GeoB6517-2 and ODP 1076D, it is likely that the recorded magnetic intensity signal is predominantly carried by the ultra-fine-grained fraction. However, the influence of other factors on the degree of alignment of magnetic particles in different grain-size fractions (e.g., sedimentation rate and clay content) cannot be quantified.

In summary, our normalized remanence records must be interpreted with caution. The two records are notably different. Comparisons with the sparse available palaeointensity information from adjacent regions and existing models suggest that the intensity signal might be recorded more reliably in core GeoB6517-2 than in core ODP 1076D. Nevertheless, further high-resolution RPI records from low latitudes and the southern hemisphere, especially from the Atlantic Ocean and surrounding regions, are needed to confirm or reject this interpretation of the normalized remanence records from cores GeoB6517-2 and ODP 1076D. However, it might require new methods to extract RPI signals from coexisting detrital and biogenic magnetic fractions in sediment records before RPI can be reliably recovered.

Conclusions

Detailed rock magnetic investigations on sediment cores GeoB6517-2 and ODP 1076D from the Congo Fan reveal a heterogeneous magnetic mineral composition, with biogenic magnetite in the SD-size range and detrital (Ti-)magnetite of varying grain sizes as the main magnetic carrier minerals. Thermomagnetic measurements allow further identification of Fe-hydroxides and pyrite, with the latter being a product of reductive diagenesis in these organic-rich sediments. Sediments older than 20 ka are affected by nearly total dissolution of the fine-grained magnetic fraction, which results in a highly scattered palaeomagnetic signal and the loss of any geomagnetic intensity information. Individual inclination and declination records obtained from cores GeoB6517-2 and ODP 1076D at ages younger than 9 and 20 ka appear reasonable. Despite having larger than expected differences for closely adjacent sites, they have similarities with other low-latitude African records. Both the biogenic and detrital (Ti-)magnetite are assumed to carry a palaeomagnetic signal that records geomagnetic field intensity variations differently, thus producing superimposed signals that cannot be separated by the rock magnetic analysis techniques applied here. Although rock magnetic results suggest that ultra-fine-grained magnetite is the principal remanence carrier in the sediments younger than 20 ka, which should provide a reasonably reliable recorder of geomagnetic field variations, the RPI results should be interpreted with caution. Our new

records contribute to, but cannot fully resolve the incoherent picture of Holocene geomagnetic field evolution in the African/southern Atlantic Ocean region. Given that only a few palaeomagnetic records from widely separated low-latitude sites are available, comparisons with the existing field models that are, consequently, sparsely constrained for that region are highly ambiguous.

Acknowledgements We thank V. Bender and W. Hale for providing access to the GeoB and IODP core repositories, respectively, at MARUM, Bremen, and T. Shanahan for providing the depth-age model for core P12 from Lake Bosumtwi, Ghana, and J. Pätzold for providing access to unpublished data sets for cores GeoB6517-2 and GeoB6518-1. We thank Andrew Roberts and an anonymous reviewer for constructive comments that improved the manuscript. This study was funded by the German Research Foundation (DFG), grants KO2870/4–1 and NO3334/8–1 to MK and NRN, within the scope of the priority program (SPP) 1488 “Planetary Magnetism”. JL holds a scholarship from the China Scholarship Council.

References

- Barletta F, St-Onge G, Channell JET, Rochon A (2010) Dating of Holocene western Canadian Arctic sediments by matching paleomagnetic secular variation to a geomagnetic field model. *Quat Sci Rev* 29:2315–2324
- Bloemendal J, Lamb B, King J (1988) Paleoenvironmental implications of rock-magnetic properties of Late Quaternary sediment cores from the eastern Equatorial Atlantic. *Paleoceanography* 3:61–87
- Blum P (1997) Physical properties handbook: a guide to the shipboard measurement of physical properties of deep-sea cores. ODP Tech Note 26, <https://doi.org/10.2973/odp.tn.26.1997>
- Bourne MD, Feinberg JF, Stafford TW Jr, Waters MR Jr, Lundellius E Jr, Forman SL (2016) High-intensity geomagnetic field ‘spike’ observed at ca. 3000 cal BP in Texas, USA. *Earth Planet Sci Lett* 442:80–92
- Channell JET, Stoner JS, Hodell DA, Charles CD (2000) Geomagnetic paleointensity for the last 100 kyr from the sub-Antarctic South Atlantic: a tool for inter-hemisphere correlation. *Earth Planet Sci Lett* 175:145–160
- Chen L, Heslop D, Roberts AP, Chang L, Zhao X, McGregor HV, Marino G, Rodriguez-Sanz L, Rohling EJ, Pälike H (2017) Remanence acquisition efficiency in biogenic and detrital magnetite and recording of geomagnetic paleointensity. *Geochem Geophys Geosys* 18:1435–1450
- Collins JA, Schefuß E, Heslop D, Mulitza S, Prange M, Zabel M, Tjallingii R, Dokken TM, Huang E, Mackensen A, Schulz M, Tian J, Zarriess M, Wefer G (2010) Interhemispheric symmetry of the tropical African rainbelt over the past 23,000 years. *Nat Geosci* 4:42–45
- Constable C, Korte M, Panovska S (2016) Persistent high paleosecular variation activity in southern hemisphere for at least 10,000 years. *Earth Planet Sci Lett* 453:78–86
- Dekkers MJ (1989) Magnetic properties of natural pyrrhotite. II. High- and low-temperature behaviour of J_{rs} and TRM as function of grain size. *Phys Earth Planet Inter* 57:266–283
- Dillon M, Bleil U (2006) Rock magnetic signatures in diagenetically altered sediments from the Niger deep-sea fan. *J Geophys Res* 111:B03105. <https://doi.org/10.1029/2004JB003540>
- Dupont LM (2008) The Congo deep-sea fan as an archive of quaternary change in Africa and the eastern Tropical South Atlantic (a review). *Extern Controls Deep-Water Depos Syst* 92:79–87

- Egli R (2004) Characterization of individual rock magnetic components by analysis of remanence curves, 1. Unmixing natural sediments. *Stud Geophys Geod* 48:391–446
- Egli R (2013) VARIFORC: an optimized protocol for calculating non-regular first-order reversal curve (FORC) diagrams. *Glob Planet Change* 110:302–320
- Egli R, Chen AP, Winklhofer M, Kodama KP, Horng CS (2010) Detection of noninteracting single domain particles using first-order reversal curve diagrams. *Geochem Geophys Geosys* 11:Q01Z11. <https://doi.org/10.1029/2009GC002916>
- Eisma D, Kalf J, Van der Gaast SJ (1978) Suspended matter in the Zaire estuary and the adjacent Atlantic Ocean. *Neth J Sea Res* 12:382–406
- Ellwood BB, Brett CE, MacDonald WD (2007) Magnetostratigraphy susceptibility of the Upper Ordovician Kope Formation, northern Kentucky. *Palaeogeogr Palaeoclimatol Palaeoecol* 243:42–54
- Frank U, Nowaczyk NR (2008) Mineral magnetic properties of artificial samples systematically mixed from haematite and magnetite. *Geophys J Int* 175:449–461
- Frank U, Nowaczyk NR, Negendank JFW, Melles M (2002a) A paleomagnetic record from Lama Lake, northern Central Siberia. *Phys Earth Planet Inter* 133:3–20
- Frank U, Nowaczyk NR, Negendank JFW (2007b) Rock magnetism of greigite bearing sediments from the Dead Sea, Israel. *Geophys J Int* 168:921–934
- Frank U, Nowaczyk NR, Frederichs T, Korte M (2017) Palaeo- and rock magnetic investigations on Late Quaternary sediments from low latitudes I: geomagnetic palaeosecular variation and relative paleointensity records from the Tobago Basin, Southeast Caribbean. *Geophys J Int* 208:1740–1755
- Gallet Y, Molist Montaña M, Genevey A, Clop García X, Thébaud E, Gómez Bach A, Le Goff M, Robert B, Nachasova I (2015) New Late Neolithic (c. 7000–5000 BC) archeointensity data from Syria. Reconstructing 9000 years of archeomagnetic field intensity variations in the Middle East. *Phys Earth Planet Inter* 238:89–103
- Hanesch M, Stanjek H, Petersen N (2006) Thermomagnetic measurements of soil iron minerals: the role of organic carbon. *Geophys J Int* 165:53–61
- Harrison RJ, Feinberg JM (2008) FORCinel: an improved algorithm for calculating first-order reversal curve distributions using locally weighted regression smoothing. *Geochem Geophys Geosys* 9:Q05016. <https://doi.org/10.1029/2008GC001987>
- Heezen BC, Menzies RJ, Schneider DE, Ewing WM, Granelli NCL (1964) Congo submarine canyon. *AAPG Bull* 48:1126–1149
- Heslop D, Dekkers MJ, Kruijver PP, Van Oorschot IHM (2002) Analysis of isothermal remanent magnetization acquisition curves using the expectation-maximization algorithm. *Geophys J Int* 148:58–64
- Hilgenfeldt K (2000) Diagenetic dissolution of biogenic magnetite in surface sediments of the Beguela upwelling system. *Int J Earth Sci* 88:630–640
- Hirt AM, Banin A, Gehring AU (1993) Thermal generation of ferromagnetic minerals from iron-enriched smectites. *Geophys J Int* 115:1161–1168
- Itambi AC, Von Dobeneck T, Mulitza S, Bickert T, Heslop D (2009) Millennial-scale northwest African droughts related to Heinrich events and Dansgaard-Oeschger cycles: evidence in marine sediments from offshore Senegal. *Paleoceanography* 24:PA1205. <https://doi.org/10.1029/2007PA001570>
- Itambi AC, Von Dobeneck T, Adegbe AT (2010) Millennial-scale precipitation changes over Central Africa during the Late Quaternary and Holocene: evidence in sediments from the Gulf of Guinea. *J Quat Sci* 25:267–279
- King JW, Banerjee SK, Marvin J (1983) A new rock-magnetic approach to selecting sediments for geomagnetic palaeointensity studies: application to palaeointensity for the last 4000 years. *J Geophys Res* 88:5911–5921
- Kirschvink JL (1980) The least-squares line and plane and the analysis of palaeomagnetic data. *Geophys J Roy Astron Soc* 62(3):699–718
- Kissel C, Rodriguez-Gonzales A, Laj C, Perez-Torrado F, Carracedo JC, Wandres C, Guillou H (2015) Paleosecular variation of the Earth magnetic field at the Canary Islands over the last 15 ka. *Earth Planet Sci Lett* 412:52–60
- Lebamba J, Vincens A, Maley J (2012) Pollen, vegetation change and climate at Lake Barombi Mbo (Cameroon) during the last ca. 33 000 cal yr. BP: a numerical approach. *Clim Past* 8:59–78
- Lund S, Platzmann E, Johnson T (2016) Full-vector paleomagnetic secular variation records from latest Quaternary sediment of lake Malawi (10.0°S, 34.3°E). *Quat Sci Rev* 144:16–27
- Marret F, Scourse J, Kennedy H, Ufkes E, Jansen JHF (2008) Marine production in the Congo-influenced SE Atlantic over the past 30,000 years: a novel dinoflagellate-cyst based transfer function approach. *Mar Micropal* 68:198–222
- Minyuk PS, Subotnikova TV, Plyaskevich AA (2011) Measurements of thermal magnetic susceptibility of hematite and goethite. *Iz Phys Solid Earth* 47:762–774
- Müller PJ (2003a) Density and water content of sediment core GeoB6517-2, PANGAEA, <https://doi.org/10.1594/PANGAEA.133967>
- Müller PJ (2003b) Density and water content of sediment core GeoB6518-1, PANGAEA, <https://doi.org/10.1594/PANGAEA.133969>
- Müller PJ (2004a) Carbon and nitrogen data of sediment core GeoB6517-2, PANGAEA, Unpublished dataset #133976
- Müller PJ (2004b) Carbon and nitrogen data of sediment core GeoB6518-1, PANGAEA, Unpublished dataset #135708
- Nilsson A, Holme R, Korte M, Suttie N, Hill M (2014) Reconstructing Holocene geomagnetic field variation: new methods, models and implications. *Geophys J Int* 198:229–248
- Nowaczyk NR (2011) Dissolution of titanomagnetites and sulphidization in sediments from Lake Kinneret, Israel. *Geophys J Int* 187:34–44. <https://doi.org/10.1111/j.1365-246X.2011.05120.x>
- Nowaczyk NR, Arz HW, Frank U, Kind J, Plessen B (2012) Dynamics of the Laschamp geomagnetic excursion from Black Sea sediments. *Earth Planet Sci Lett* 351–352:54–69
- Nowaczyk NR, Frank U, Kind J, Arz HW (2013) A high-resolution paleointensity stack from 14 to 68 ka from Black Sea sediments. *Earth Planet Sci Lett* 384:1–16
- Ouyang T, Heslop D, Roberts AP, Tian C, Zhu Z, Qiu Y, Peng X (2014) Variable remanence acquisition efficiency in sediments containing biogenic and detrital magnetites: implications for relative paleointensity signal recording. *Geochem Geophys Geosys* 15:2780–2796
- Passier HF, de Lange GJ, Dekkers MJ (2001) Magnetic properties and geochemistry of the active oxidation front and the youngest sapropel in the eastern Mediterranean Sea. *Geophys J Int* 145:604–614
- Paterson GA, Wang Y, Pan Y (2013) The fidelity of paleomagnetic records carried by magnetosome chains. *Earth Planet Sci Lett* 383:82–91
- Peck JA, Green RR, Shanahan T, King JW, Overpeck JT, Scholz CA (2004) A magnetic mineral record of Late Quaternary tropical climate variability from Lake Bosumtwi, Ghana. *Palaeogeogr Palaeoclimatol Palaeoecol* 215:37–57
- Petermann H, Bleil U (1993) Detection of live magnetotactic bacteria in South Atlantic deep-sea sediment. *Earth Planet Sci Lett* 117:223–228
- Roberts AP, Pike CR, Verosub KL (2000) First-order reversal curve diagrams: a new tool for characterizing the magnetic properties of natural samples. *J Geophys Res* 105:28461–28475
- Roberts AP, Chang L, Heslop D, Florindo F, Larrasoana JC (2012) Searching for single domain magnetite in the “pseudo-single-domain” sedimentary haystack: implications of biogenic magnetite preservation for sediment magnetism and relative

- paleointensity determinations. *J Geophys Res* 117:B08104. <https://doi.org/10.1029/2012JB009412>
- Roberts AP, Almeida TP, Church NS, Harrison RJ, Heslop D, Li Y, Li J, Muxworthy AR, Williams W, Zhao X (2017) Resolving the origin of pseudo-single domain magnetic behaviour. *J Geophys Res* 122:9534–9558
- Rochette P, Fillion G (1989) Field and temperature behaviour of remanence in synthetic goethite: paleomagnetic implications. *Geophys Res Lett* 16:851–854
- Rochette P, Mathé PE, Esteban L, Rakoto H, Bouchez J-L, Liu Q, Torrent J (2005) Non-saturation of the defect moment of goethite and fine-grained hematite up to 57 Teslas. *Geophys Res Lett* 32:L22309. <https://doi.org/10.1029/2005GL024196>
- Rowan CR, Roberts AP, Broadbent T (2009) Reductive diagenesis, magnetite dissolution, greigite growth and paleomagnetic smoothing in marine sediments: a new view. *Earth Planet Sci Lett* 277:223–235
- Schefuß E, Schouten S, Schneider RR (2005) Climatic controls on central African hydrology during the past 20,000 years. *Nature* 437:1003–1006
- Schefuß E, Eglinton TJ, Spencer-Jones CL, Rullkötter J, De Pol-Holz R, Talbot HM, Grootes PM, Schneider RR (2016) Hydrologic control of carbon cycling and aged carbon discharge in the Congo River basin. *Nat Geosci* 9:687–690
- Schwartz M, Lund SP, Hammond DE, Schwartz R, Wong K (1997) Early sediment diagenesis on the Blake/Bahama Outer Ridge, North Atlantic Ocean and its effects on sediment magnetism. *J Geophys Res* 102:7903–7914
- Shanahan TM, Beck JW, Overpeck JT, McKay NP, Pigati JS, Peck JA, Scholz CA, Heil Jr CW, King J (2012) Late Quaternary sedimentological and climate changes at Lake Bosumtwi Ghana: new constraints from laminae analysis and radiocarbon age modeling. *Palaeogeogr Palaeoclim Palaeoecol* 316:49–60
- Spieß V, Cruise P (2002) METEOR Cruise No. 47. Leg 3, 1 June–3 July 2000. Libreville—Walvis Bay, Institut für Meereskunde der Universität, Hamburg
- Stoner JS, Laj C, Channell JET, Kissel C (2002) South Atlantic and North Atlantic geomagnetic paleointensity stacks (0–80 ka): implications for inter-hemispheric correlation. *Quat Sci Rev* 21:1141–1151
- Stoner JS, Channell JET, Hodell DA, Charles CD (2003) A ~ 580 kyr paleomagnetic record from the sub-Antarctic South Atlantic (Ocean Drilling Program site 1089). *J Geophys Res* 108:2244
- Tauxe L (1993) Sedimentary records of relative paleointensity of the geomagnetic field: theory and practice. *Rev Geophys* 31:319–354
- Thouveny N, Williamson D (1988) Palaeomagnetic study of the Holocene and Upper Pleistocene sediments from Lake Barombi Mbo, Cameroun: first results. *Phys Earth Planet Inter* 52:193–206
- Van Vreumingen MJ (1984) A palaeomagnetic and rockmagnetic study of sediment cores from the Zaire Submarine Fan. *Neth J Sea Res* 17:342–363
- Walker B (2001) High-resolution paleomagnetic analysis of a sediment core from Lake Bosumtwi, Ghana. in GSO Technical Report No. 2001-2, University of Rhode Island, Rhode Island, 46–56
- Wefer G, Shipboard Scientific Party (1998a) Leg 175 Introduction. In Proc. ODP Init. Repts., 175, eds. Wefer, G, Berger, WH, Richter, C et al., Ocean Drilling Program, College Station, TX, 7–25
- Wefer G, Berger WH, Richter C, Shipboard Scientific Party (1998a) Facies pattern and authigenic minerals of upwelling deposits off southwest Africa. In: Proc. ODP Init. Repts., 175, Wefer G, Berger WH, Richter C (eds) Ocean drilling program, College Station, TX, 487–504
- Wefer G, Shipboard Scientific Party (1998b) Site 1076. In: Proc. ODP Init. Repts., 175, Wefer G, Berger WH, Richter C (eds) Ocean drilling program, College Station, TX, 87–113
- Weijers JWH, Schouten S, Schefuß E, Schneider RR, Damstè JSS (2009) Disentangling marine, soil and plant organic carbon contributions to continental margin sediments: a multi-proxy approach in a 20,000 year sediment record from the Congo deep-sea fan. *Geochim Cosmochim Acta* 73:119–132